Modeling and Control of an Axial Bearing Generating Forces and Torques

C. Klaucke, St. Eckhardt and J. Rudolph
Technische Universität Dresden
Institut für Regelungs- und Steuerungstheorie
01062 Dresden, Germany
{*carsten.klaucke, stephan.eckhardt, joachim.rudolph*}*@tu-dresden.de*

***Abstract*— A new type of active axial magnetic bearing is considered which is capable of generating forces and torques. A network approach is used for modeling of the position dependent current-force/torque-relation. The bearing is used for positioning with a flatness-based position controller. Results from model validation and position control experiments are presented.**

I. Introduction

Magnetically levitated shafts can be used for machine tool spindles in order to produce circular and non-circular holes with high precision. A typical set-up of such a tooling spindle uses two electro-magnetic radial bearings, one electro-magnetic axial bearing, and a motor which generates the driving torque. A lower number of bearings or a more compact design are possible using bearingless motors. Instead, in this contribution we propose to use an adapted axial bearing that generates both levitation forces and torques. This forms an alternative for reducing the construction by one radial bearing.

The known self-bearing disc motor construction (see for instance [1]) has been modified. The resulting axial bearing consists of two similar parts capable to generate torques and axial forces. Each of the parts is made of a cylindrical core with radial slots. One, thus, has a stator core with salient trapezoidal poles that are equipped with the coils (Fig. 1). As opposed to a disc motor design, here the bearing disc does not carry permanent magnets.

The spatial distribution of the poles allows one to generate forces and torques acting on the disc. Roughly, the forces are used for axial positioning while the torques are used to replace, or to increase, forces that would else be generated by a radial bearing.

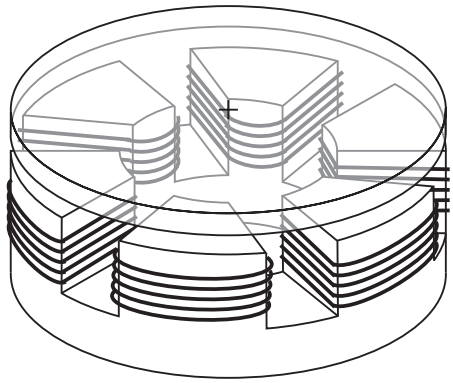

Fig. 1. Schematic drawing of one half of the axial bearing and the bearing disc (semi-transparent).

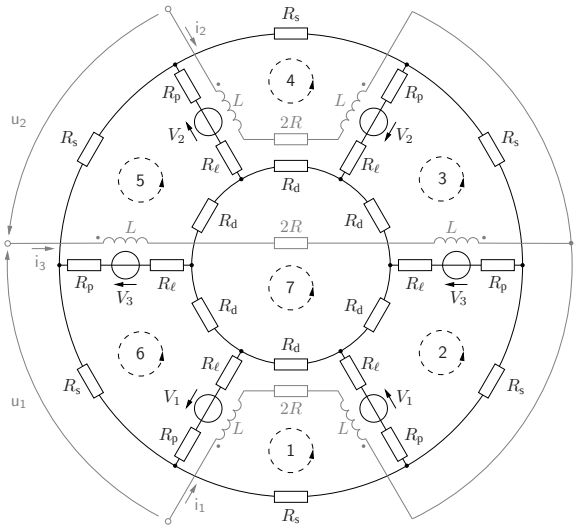

Fig. 2. Electrical (light) and magnetical (dark) network of one half of the axial bearing with one possible Y-connection.

With this new configuration the equations of the rigid-body motion of the shaft are simplified, and lead to decoupled equations for forces and torques. A flatness based controller can be designed, extending work of [2], [3].

II. Modeling and Control

In this section the modeling of the axial bearing is discussed. The calculation of the forces and torques is based on a network approach. For a particular Y-connection an approach is presented that allows us to obtain a relation between forces/torques and currents depending on the position. This model can be used to calculate the control currents realizing forces and torques required by a position controller. At the end of the section a short summary of the flatness-based position controller used is given.

A. Axial bearing setup

We consider an axial bearing consisting of two six-pole halves, where each pole is provided with a coil of w windings and a bearing disc (see Fig. 1). In order to obtain

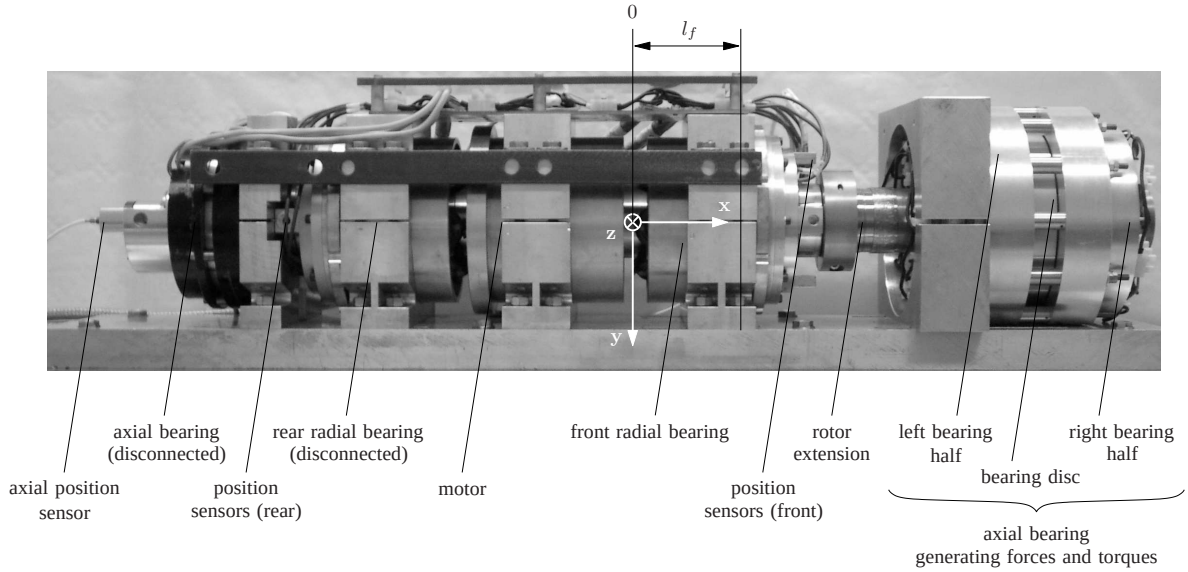

Fig. 3. Photograph of the laboratory spindle used for experiments.

the per pole magnetic flux in the air gap we consider a magnetic network of the axial bearing half. If we assume linear magnetic characteristics of the material and neglect leakage fluxes we get a magnetic network as depicted in Fig. 2 (dark circuit); concerning the use of network models see also [5]. The magnetic resistances of the stator and the disc are related to the geometric dimensions:

$$R_{\mathrm{m}} = \frac{\ell}{\mu A}$$

Here ℓ is the extent of the magnetizable material in field direction, A the relevant cross-sectional area perpendicular to the field direction, and μ the permeability of the magnetizable material. For the network approach we introduce four magnetic resistances: the magnetic resistance R_{d} of a disc sector (angle $\pi/3$), the magnetic resistance R_{s} of a sector of the stator base (angle $\pi/3$), the magnetic resistance R_{p} of a pole, and the magnetic resistance R_ℓ of the air gap with length ℓ_{gap} between one pole and the disc. For the sake of simplicity, we assume that the bearing disc and the stator plane are parallel. Thus, the length of the air gap is the same for all poles of one bearing half.

Since the coils need not be connected in a particular way, we can analyze different configurations. A first useful possibility is to connect two adjacent coils in series, thus, obtaining three coil pairs per half. This configuration requires a six channel power amplifier. An alternative is to connect two opposite coil pairs in series and then connect them in Y with the remaining coils, so that $i_3 = -i_1 - i_2$ (see the light circuit in Fig. 2). The main difference between those two connections is the following. A bearing half can generate torques about two axes with the first connection and about one axis only with the second connection, assuming that the bearing is properly aligned. However, this is not a disadvantage of the Y-connection, because a second half is always needed in oder to generate positive and negative axial forces. Torques about two axes can be generated if the two halves are mounted with a $\pi/2$ turn w.r.t. one other. The main advantages of the Y-connection are that DC-voltage link inverters can be used and that simpler equations for the current-force/torque-relations can be obtained.

B. Experimental set-up

The laboratory test-bench is shown in Fig. 3. The conventional axial bearing and the rear radial bearing were disconnected but not removed (see Fig. 3). Furthermore, a rotor extension carries an axial bearing disc. The two axial bearing halves are placed on the left and on the right of the bearing disc. Indeed, this set-up does not benefit from the possibility of reducing the set-up by one radial bearing. Rather, it just allows us to show the feasibility of magnetic levitation with the new axial bearing. In order to benefit from reducing the set-up by one radial bearing a new rotor with a shorter length can be used. This will reduce the total length of the spindle and yield a more compact design.

C. Equations of the rigid body dynamics

As one radial bearing is removed, the equations of the rigid-body model of the spindle used in [4] must be adapted. Instead of having four radial forces (each radial bearing with a force in y- and z-direction) and one axial force, there are two radial forces, two torques (about the y- and z-axis), and one axial force. This leads to decoupled equations for forces and torques, which can be written as follows (gyroscopic forces neglected):

$$m\ddot{X} = F_x + mg_x \tag{1a}$$
$$m\ddot{Y} = F_y + mg_y \tag{1b}$$
$$m\ddot{Z} = F_z + mg_z \tag{1c}$$
$$J_2\ddot{\psi} = M_y - l_f F_z \tag{1d}$$
$$J_2\ddot{\theta} = M_z + l_f F_y \tag{1e}$$
$$J_1\ddot{\varphi} = D_\varphi \tag{1f}$$

Using the inertial coordinate system given in Fig. 3, we denote the Cartesian coordinates of the center of mass as X, Y, Z and the Bryant angles as φ, ψ, and θ. The parameter l_f denotes the distance between the radial bearing and the center of mass (see Fig. 3). Finally, F_y, F_z are the radial forces, F_x is the axial force and M_y, M_z are the torques about the y- and z-axis, respectively. The mass of the rotor is denoted as m, the components of the gravitational acceleration vector as g_x, g_y, g_z, and the moments of inertia of the symmetric rotor are J_1, J_2, where $J_2 > J_1$. The driving torque is D_φ.

At this point we can also define the length of the air gap using the coordinates. For the left and the right side of the bearing disc, we respectively get

$$\ell_{\text{gap}} = \ell_0 \pm X$$

with the nominal air gap length ℓ_0.

D. Modeling the current-force/torque-relation with a network approach for one bearing half

The Y-connection shown in Fig. 2 cannot be simplified to single horseshoe magnets in order to get a decoupled model. This is due to the windings of the third phase, which lead to non-negligible magnetic fluxes through adjacent poles. In order to obtain equations for the current-force/torque-relation, first the network in Fig. 2 is used to describe the magnetic fluxes in the air gaps w.r.t. the currents:

$$\Phi_\ell = \frac{w}{\mathcal{N}} \begin{pmatrix} R_1 & R_2 \\ -R_1 & -R_2 \\ R_3 & R_3 \\ -R_2 & -R_1 \\ R_2 & R_1 \\ -R_3 & -R_3 \end{pmatrix} \begin{pmatrix} i_1 \\ i_2 \end{pmatrix} \tag{2}$$

where w denotes the windings of one coil and

$$\begin{aligned} \mathcal{N} &= \prod_{\nu \in \{1,3,4\}} \Big(R_\text{s} + R_\text{d} + \nu(R_\text{p} + R_\ell) \Big) \\ R_1 &= 4(R_\text{s} + R_\text{d})^2 + 12(R_\text{p} + R_\ell)^2 \\ &\quad + 17(R_\text{p} + R_\ell)(R_\text{s} + R_\text{d}) \\ R_2 &= (2R_\ell + 2R_\text{p} + R_\text{d} + R_\text{s})(R_\text{s} + R_\text{d}) \\ R_3 &= (R_\text{s} + R_\text{d} + 3R_\text{p} + 3R_\ell) \\ &\quad \times (3R_\text{s} + 3R_\text{d} + 4R_\text{p} + 4R_\ell) \end{aligned}$$

With the six air gap flux components of Φ_ℓ in (2) one can calculate the forces and torques, which depend on the mounting angle. As mentioned above, the halves are rotated by an angle of 90° w.r.t. one another. Here the half left from the bearing disc (in Fig. 3) is considered. The axial force acts in negative x-direction and is modeled as

$$\begin{aligned} F_{x,-} = c_F \big[&\left(i_1^2 + i_2^2\right)\left(2R_1^2 + 2R_2^2 + 2R_3^2\right) \\ &+ i_1 i_2 \left(8R_1R_2 + 4R_3^2\right) \big] \end{aligned} \tag{3}$$

The torques are given by

$$M_y \equiv 0 \tag{4}$$

$$M_z = \sqrt{3} r_F c_F \left(i_1^2 - i_2^2\right)\left(R_1^2 - R_2^2\right) \tag{5}$$

with $c_F = w^2/(2\mu_0 A_\text{p} \mathcal{N}^2)$, where A_p is the cross-sectional area of a pole and r_F the radial distance between the center of the disc and the point where the resulting force is assumed to be applied. Our aim is to get the current-force/torque-relation. However, it is difficult to get explicit expressions for i_1 and i_2 from the equations above. One approach is to use a coordinate transformation in order to simplify the equations, as follows.

Looking at (3) and (5) one may observe that the equations for the forces and for the torques describe ellipses and hyperbolas, respectively (see also Fig. 4). Rotating the i_1-i_2-coordinate system about $\pi/4$ and introducing the transformed currents $\tilde{i}_1, \tilde{i}_2$ the mixed term in the expression for the force $F_{x,-}$ in (3) vanishes:

$$F_{x,-} = 2c_F \left[(R_1 - R_2)^2 \tilde{i}_1^2 + ((R_1 + R_2)^2 + 2R_3^2) \tilde{i}_2^2 \right]$$

Moreover, the equation for the torque M_z in (5) simplifies to

$$M_z = 2\sqrt{3} r_F c_F (R_1^2 - R_2^2) \tilde{i}_1 \tilde{i}_2$$

If we keep in mind that electromagnets can generate attracting forces ($F_{x,-} \geq 0$) only, we can find up to four solutions for $\tilde{i}_1$ and $\tilde{i}_2$. For $F_{x,-} \to \infty$ the first pair of solutions approaches the $\tilde{i}_1$-axis:

$$\begin{aligned} \tilde{i}_1 &= \frac{\varepsilon}{\sqrt{8\sqrt{3} c_F^2 r_F (R_1 - R_2)^3 (R_1 + R_2)}} \\ \tilde{i}_2 &= \sqrt{\frac{2(R_1 - R_2)}{\sqrt{3} r_F (R_1 + R_2)}} \frac{M_z}{\varepsilon} \end{aligned}$$

while the second pair of solutions approaches the $\tilde{i}_2$-axis:

$$\begin{aligned} \tilde{i}_1 &= \sqrt{\frac{2((R_1 + R_2)^2 + 2R_3^2)}{\sqrt{3} r_F (R_1^2 - R_2^2)}} \frac{M_z}{\varepsilon} \\ \tilde{i}_2 &= \frac{\varepsilon}{\sqrt{8\sqrt{3} c_F^2 r_F ((R_1 + R_2)^2 + 2R_3^2)(R_1^2 - R_2^2)}} \end{aligned}$$

Here ε is given by

$$\begin{aligned} \varepsilon = \pm &\sqrt{F_{x,-} + \sqrt{F_{x,-}^2 - \frac{4\big((R_1 + R_2)^2 + 2R_3^2\big) M_z^2}{3 r_F^2 (R_1 + R_2)^2}}} \\ &\times \sqrt{2\sqrt{3} r_F c_F (R_1^2 - R_2^2)} \end{aligned}$$

The sign of ε determines the solution quadrant in the transformed coordinate system. When a torque is generated also an axial force is produced. Thus, we obtain

$$F_{x,-}^M = \sqrt{\frac{4\big((R_1 + R_2)^2 + 2R_3^2\big) M_z^2}{3 r_F^2 (R_1 + R_2)^2}}$$

To get real solutions for ε we have to satisfy $F_{x,-} \geq F_{x,-}^M$. Finally, the original current components result from the inverse coordinate transformation as

$$\begin{pmatrix} i_1 \\ i_2 \end{pmatrix} = \frac{1}{\sqrt{2}} \begin{pmatrix} \tilde{i}_1 + \tilde{i}_2 \\ -\tilde{i}_1 + \tilde{i}_2 \end{pmatrix}$$

E. Model equations of a complete axial bearing

So-far we discussed the left axial bearing half only. For the complete model we also need the equations for the right half. The fact that the left and the right half are geometrically and electrically similar, but mounted under a different angle permits us to re-use the equations given above with the following adaptations. First we have to use $\ell_0 - X$ instead of $\ell_0 + X$ for the air gap length ℓ_{gap}. This affects R_ℓ and, thus, the abbreviations $\mathcal{N}, R_1, R_2, R_3$ and c_F. Then we have to substitute the currents i_1, i_2, and i_3 with the corresponding currents i_4, i_5, and i_6. Furthermore, the different mounting angle and position of the bearing half affects the direction of the axial force, which acts in positive x-direction and is, therefore, denoted by $F_{x,+}$. Finally, the expressions for the torques M_y and M_z must be interchanged (now $M_z \equiv 0$).

With the resulting axial force

$$F_x = F_{x,+} - F_{x,-}$$

we now have a set of equations which describe the position dependent current-force/torque-relation of the complete axial bearing. The magnetic coupling of the two halves can be neglected due to the design of the bearing disc.

In order to calculate the currents required for generating forces and torques we have to determine the axial forces for both halves. If we introduce F_0 as a positive bias force and $F_{x,d}$ as a desired axial force, we obtain

$$F_{x,+,d} = \begin{cases} F_{x,d} + F_{x,-}^M + F_0 & \text{if} \quad F_{x,d} \geq F_x^M \\ F_{x,+}^M + F_0 & \text{if} \quad F_{x,d} < F_x^M \end{cases}$$

$$F_{x,-,d} = \begin{cases} F_{x,-}^M + F_0 & \text{if} \quad F_{x,d} \geq F_x^M \\ -F_{x,d} + F_{x,+}^M + F_0 & \text{if} \quad F_{x,d} < F_x^M \end{cases}$$

where

$$F_x^M = F_{x,+}^M - F_{x,-}^M$$

is the resulting force produced when generating the desired torques $M_{y,d}$ and $M_{z,d}$.

F. Position control with one axial and one radial magnetic bearing

As discussed in [4], the controller has a cascade structure. The inner controller is the current controller. In the case of the axial bearing current control is done by the controller of the DC-voltage link converter. The outer controller is a flatness-based position tracking controller, which generates control forces and torques. The control currents can be calculated with the position dependent current-force/torque-relation obtained above.

The position controller was designed using the position and orientation of the rigid body as components of a flat output. Thus, only the equations (1) for the rigid body dynamics must be adapted, while all the other controller equations remain unchanged.

III. Experimentation

The models derived were validated using a bearing test-bench conceived for this purpose. It allows us to freely position the rotor in the air gap of the bearing. While the position is fixed, an appropriate number of current-pairs are generated and the resulting forces are measured. Measurement data thus obtained can be used to validate the mathematical models and to identify model parameters.

For the position control we used the experimentation set-up with the modifications discussed in the previous section (see Fig. 3). The algorithms for the position control were implemented on a dSPACE DS1103 controller board. For the radial bearing a power amplifier with duty ratio inputs was used and for the axial bearing we used two DC-voltage link converters with current control.

A. Experimental identification of the current-force/torque-relation

The position dependent current-force/torque-relation for the axial bearing was measured for different electrical connections. One experimental result with the Y-connection given in Fig. 2 is reported on Fig. 4. The mathematical model with the identified parameters is shown in this figure, too. One may observe a good fitting of model and experimentation data.

Comparing the calculated with the measured iso-lines one may see that the assumption of linear magnetic behavior holds in a limited area. For high currents saturation of forces and torques occurs. Thus, the linear model is not valid at high currents. This is especially true for the torques.

B. Results of the position control experiments

Experimentation was done at standstill, because the expected unbalance of the modified rotor would not allow rotations at higher speed. However, it is possible to simulate a rotation, i.e., instead of measuring the angle φ it is computed for a given speed.

We considered an elliptic path with major axis $r_y = 20\,\mu\text{m}$ and minor axis $r_z = 10\,\mu\text{m}$. The shaft central axis follows the path periodically 2000 times a minute (as would be required in a synchronized motion at 2000 rpm). We used a flatness-based control for the position of the center of mass and the orientation of the rotor as discussed in [4]. Fig. 5 shows the control force and torques. In Fig. 6 the corresponding control currents of both axial bearing halves are given. The desired and measured positions in the two measurement planes are reported in Fig. 7.

IV. Conclusion

A new axial bearing which is capable of generating forces and torques was introduced. The prototype used for the measurements demonstrates the feasibility of a magnetically levitated shaft with one radial and one axial bearing in Y-connection. If a shorter rotor is used, one can fully benefit of the advantages of the new axial bearing, which renders a more compact design possible.

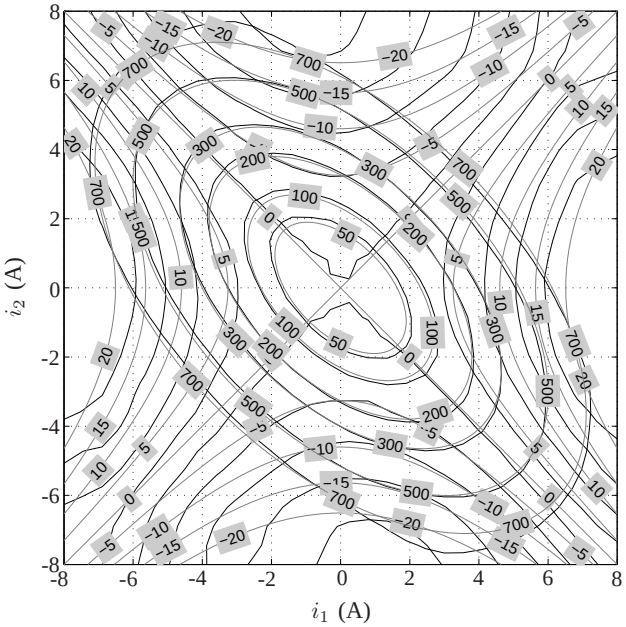

Fig. 4. Iso-lines for forces (ellipses) and torques (hyperbolas) as functions of coil currents at nominal air gap; measurements (dark) versus mathematical model (light).

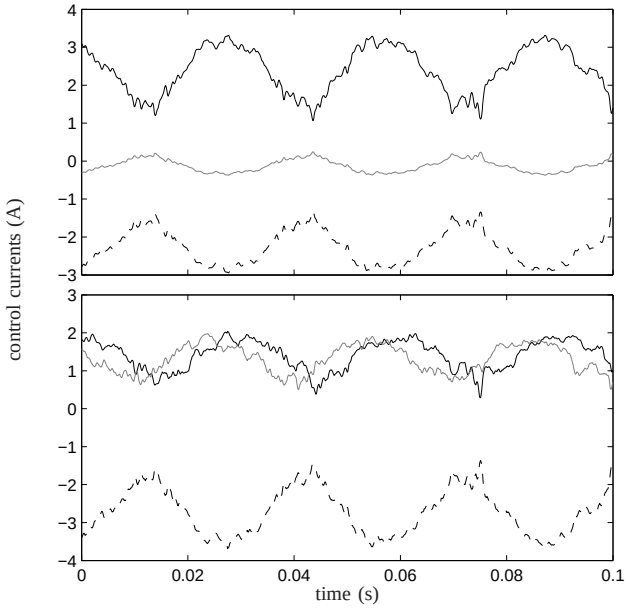

Fig. 6. Control currents i_1 (dark), i_2 (light), i_3 (dashed) in the upper plot for the left axial bearing half and i_4 (dark), i_5 (light), i_6 (dashed) in the lower plot for the right axial bearing half.

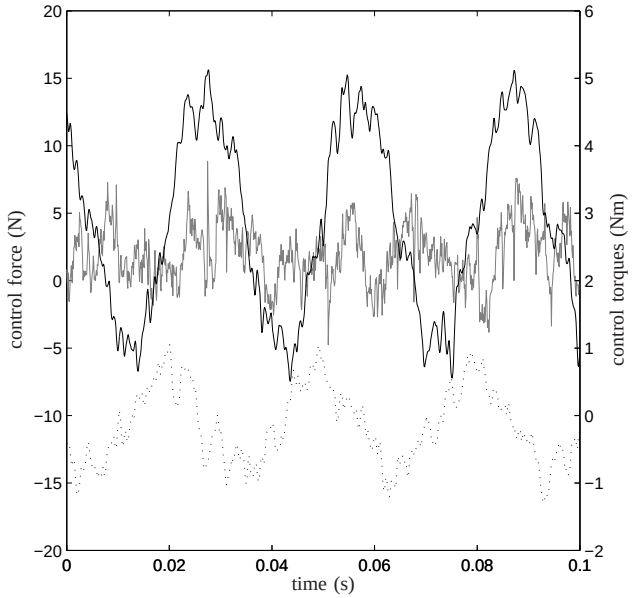

Fig. 5. Control force F_x (light) and torques M_y (dotted) and M_z (dark) for the axial bearing.

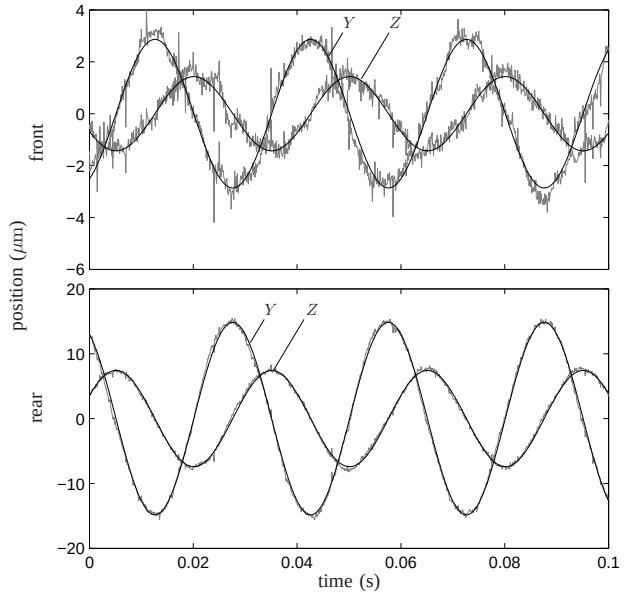

Fig. 7. Measured (light) and desired (dark) position in the two measurement planes.

ACKNOWLEDGMENT

This work has been partially supported by the German government (BMWi) in the frame of the InnoNet project PreciGrind.

REFERENCES

[1] S. Ueno, and Y. Okada. Characteristics and Control of a Bidirectional Axial Gap Combined Motor-Bearing. *IEEE Trans. Mechatronics*, 5:310–318, 2000.

[2] J. Lévine, J. Lottin, and J.-C. Ponsart. A nonlinear approach to the control of magnetic bearings. *IEEE Trans. Contr. Syst. Technol.*, 4:524–545, 1996.

[3] J. v. Löwis, J. Rudolph, J. Thiele, and F. Urban. Flatness-based trajectory tracking control of a rotating shaft. In *7th International Symposium on Magnetic Bearings, Zürich*, pp. 299–304, 2000.

[4] St. Eckhardt, and J. Rudolph. High Precision Synchronous Tool Path Tracking with an AMB Machine Tool Spindle. In *9th International Symposium on Magnetic Bearings, Lexington*, paper no. 109, 2004.

[5] C. Collon, S. Eckhardt and J. Rudolph. A Network Approach to the Modeling of Active Magnetic Bearings. In *Proc. 5th MATHMOD Vienna*, CD-ROM, pp. 3-1 - 3-10, 2006.